PERGAMON

Acta mater. 48 (2000) 2383–2398

Acta MATERIALIA

www.elsevier.com/locate/actamat

QUASI-STATIC AND DYNAMIC MECHANICAL RESPONSE OF *HALIOTIS RUFESCENS* (ABALONE) SHELLS

R. MENIG[1], M. H. MEYERS[2], M. A. MEYERS[3]† and K. S. VECCHIO[3]

[1]Institute for Materials Science I, University of Karlsruhe (TH), Germany, [2]Gen-Probe, San Diego, USA and [3]Department of Mechanical and Aerospace Engineering, University of California, San Diego, Mail Code 0411, 9500 Gilman Drive, La Jolla, CA 92093-0411, USA

(Received 7 April 1999; accepted 23 November 1999)

Abstract—Quasi-static and dynamic compression and three-point bending tests have been carried out on *Haliotis rufescens* (abalone) shells. The mechanical response of the abalone shell is correlated with its microstructure and damage mechanisms. The mechanical response is found to vary significantly from specimen to specimen and requires the application of Weibull statistics in order to be quantitatively evaluated. The abalone shell exhibited orientation dependence of strength, as well as significant strain-rate sensitivity; the failure strength at loading rates between 10×10^3 and 25×10^3 GPa/s was approx. 50% higher than the quasi-static strength. The compressive strength when loaded perpendicular to the shell surface was approx. 50% higher than parallel to the shell surface. The compressive strength of abalone is 1.5–3 times the tensile strength (as determined from flexural tests), in contrast with monolithic ceramics, for which the compressive strength is typically an order-of-magnitude greater than the tensile strength. Quasi-static compressive failure occurred gradually, in a mode sometimes described as "graceful failure". The shear strength of the organic/ceramic interfaces was determined to be approx. 30 MPa by means of a shear test. Considerable inelastic deformation of the organic layers (up to a shear strain of 0.4) preceded failure. Crack deflection, delocalization of damage, plastic microbuckling (kinking), and viscoplastic deformation of the organic layers are the most important mechanisms contributing to the unique mechanical properties of this shell. The plastic microbuckling is analysed in terms of the equations proposed by Argon (*Treatise of Materials Science and Technology*. Academic Press, New York, 1972, p. 79) and Budiansky (*Comput. Struct.* 1983, **16**, 3).

1. INTRODUCTION

The study of materials that have evolved through millions of years of evolution and natural selection can provide insights into heretofore-unexploited mechanisms of toughening. Biomimetics is a newly emerging interdisciplinary field in materials science and engineering and biology, in which lessons learned from biology form the basis for novel material concepts [1, 2]. This new field of biomimetics investigates biological structures, establishing relationships between properties and structures in order to develop methods of processing and microstructural design for new materials [1].

Many properties of biological systems are far beyond those that can be achieved in synthetic materials with present technology [3]. Biological organisms produce complex composites that are hierarchically organized in terms of composition and microstructure, containing both inorganic and organic components in complicated mixtures [4, 5]. These totally organism-controlled materials are synthesized at ambient temperature and atmospheric conditions. The unique microstructures in biological composites and the resulting properties have been, until recently, unknown to materials scientists, but are now beginning to stimulate creativity in the development of future synthetic materials.

The objectives of this work are to evaluate the static and dynamic response and evolution of damage in abalone (*Haliotis rufescens*). It is already known that the mechanical properties of these "composite" shells are outstanding, if one considers their weak constituents, namely calcium carbonate ($CaCO_3$) and a series of organic binders [6, 7]. These mollusks owe their extraordinary mechanical properties to a hierarchically organized structure, starting with single crystals of $CaCO_3$, with dimensions of 4–5 nm (nanostructure), proceeding to "bricks" with dimensions of 0.5–10 μm (microstructure), and culminating in layers approx. 0.2 mm (mesostructure). However, to date their dynamic properties have not been established, and previous mechanical testing has been restricted to three- and four-point bending. Little is known about the mech-

† To whom all correspondence should be addressed.

1359-6454/00/$20.00
PII: S1359-6454(99)00443-7

anisms of compressive failure, as well as about the effect of loading rate on their response.

2. MOLLUSK SHELLS

Mollusk shells consist of a proteinaceous matrix in which one or more ceramic phases are embedded [8–10]. These ceramic phases, i.e. calcium carbonate ($CaCO_3$), are not suitable as structural materials because of their brittleness. However, mollusks are known to possess hierarchical structures highly optimized for toughness. These weak constituents, calcium carbonate and a series of organic binders, assembled in a hierarchical fashion, provide the mollusk shells with outstanding mechanical properties. Five main types of mollusk shell materials have been identified: prismatic (polygonal columns); foliated (long thin crystals in overlapping layers); homogeneous (fine-scale rubble); nacreous (flat tables); and crossed lamellar (plywood-like), which can occur alongside each other. The nacreous structure occurs in *H. rufescens* (red abalone) and the crossed-lamellar structure in *Strombus gigas* (pink conch).

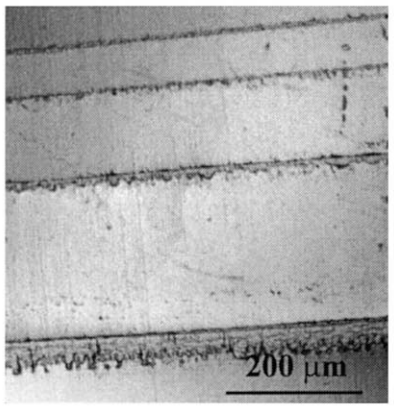

(a)

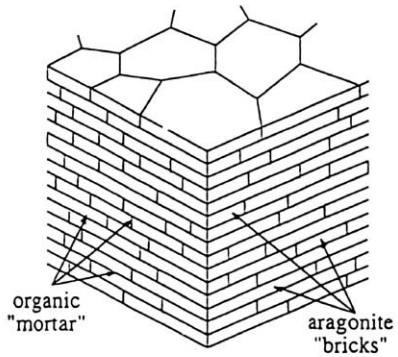

(b)

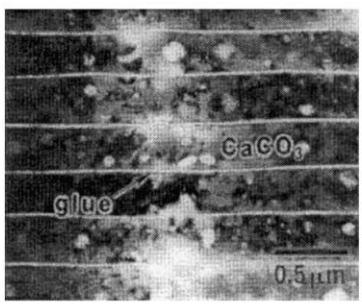

(c)

Fig. 1. (a) Optical micrograph of cross-section of abalone shell, showing mesolayers, (b) brick and mortar microstructure of nacre (schematically) [1]; (c) TEM micrograph of layered structure of abalone.

2.1. H. rufescens *(abalone shell)*

The longitudinal cross-section of the abalone shell (*H. rufescens*) shows two types of microstructure: an outer prismatic layer (calcite); and an inner nacreous layer (aragonite). The two forms of $CaCO_3$, calcite (rhombohedral) and aragonite (orthorhombic) constitute the inorganic component of this ceramic/organic composite (95 wt% ceramic, 5 wt% organic material). The nacreous layer provides an excellent combination of mechanical properties as a result of its highly ordered hierarchical structure. Nacre is composed of stacked platelets (0.2–0.5 μm thick), arranged in a so-called brick and mortar microstructure with an organic matrix (20–30 nm thickness) serving as glue between the individual platelets [11]. Figure 1(a) shows the structure of the nacre region at low magnification. Figure 1(b) shows schematically the brick and mortar microstructure, identified by Sarikaya [1], and Fig. 1(c) shows an electron micrograph of the layered structure. Two types of structure are seen in Fig. 1: the thick layers (mesolayers) which are approx. 300 μm thick are separated by layers of viscoplastic material with a thickness of about 20 μm [Fig. 1(a)]. At a smaller scale the mesolayers are comprised of "bricks" approx. 0.5 μm thick [Figs 1(b) and (c)]. Thin organic layers ("glue") separate each of these "bricks". Sarikaya *et al.* [12] conducted mechanical tests on *H. rufescens* (red abalone) and obtained a fracture strength of 185 ± 20 MPa (in bending tests) and a fracture toughness of 8 ± 3 MPa $m^{1/2}$. The scatter was explained by the natural defects in the nacre and the somewhat curved shape of the layers.

Jackson *et al.* [11] performed measurements of three mechanical properties of nacre: Young's modulus; tensile strength; and fracture toughness. The nacre was taken from the shell of a bivalve mollusk, Pinctata. They report a Young's modulus of

approx. 70 GPa for dry and 60 GPa for wet samples; the tensile strength of nacre was 170 MPa for dry and 140 MPa for wet samples. The work of fracture varied from 350 to 1240 J/m^2, depending on the span-to-depth ratio and the degree of hydration: wet nacre showing superior toughness by associated introduction of plastic work. In contrast, monolithic $CaCO_3$ showed a work of fracture that was about 3000 times less than that of the composite nacre material [13]. Jackson *et al.* [11] concluded that water affects the Young's modulus and tensile strength by reducing the shear modulus and shear strength of the organic matrix. The toughness is enhanced by water, which plasticizes the organic matrix resulting in a greater crack blunting and deflection ability. In contrast with more traditional brittle ceramics, such as Al_2O_3, or high toughness ceramics, such as ZrO_2, the crack propagation behavior in nacre reflects its highly anisotropic structure leading to a high degree of crack tortuosity [1]. Jackson *et al.* [11] concluded that the increased path length of the cracks is responsible for enhanced work of fracture. Sarikaya *et al.* [12,14] proposed several toughening mechanisms: (a) crack blunting/branching/deflection; (b) microcrack formation; (c) plate pullout; (d) crack bridging (ligament formation); and (e) sliding of $CaCO_3$ layers. The high degree of crack tortuosity in these shells may be due mainly to crack blunting and branching. Meyers [15] also observed crack deflection at the mesolayers, which have thick (20 μm) organic interfaces.

3. EXPERIMENTAL APPROACH

The shells studied herein were purchased at a local shell shop (La Jolla, CA) in a dry condition. All abalone samples were cut out of the same specimen to minimize varying test results due to differences in shell history or age. The abalone belonged to the "red" family. The first cuts were made by hand, using a hacksaw with an abrasive blade. After obtaining pieces of appropriate size, a high-speed diamond saw was used for further sectioning. Long flat areas with a minimum length of 40 mm and cross-sectional areas of about 5 mm × 5 mm were kept for producing three-point bend samples. Care was taken to obtain parallel sides and 90°-angles and also to mark the side of the exterior layer.

3.1. Compression and shear testing

The compression test samples were cut to cubes

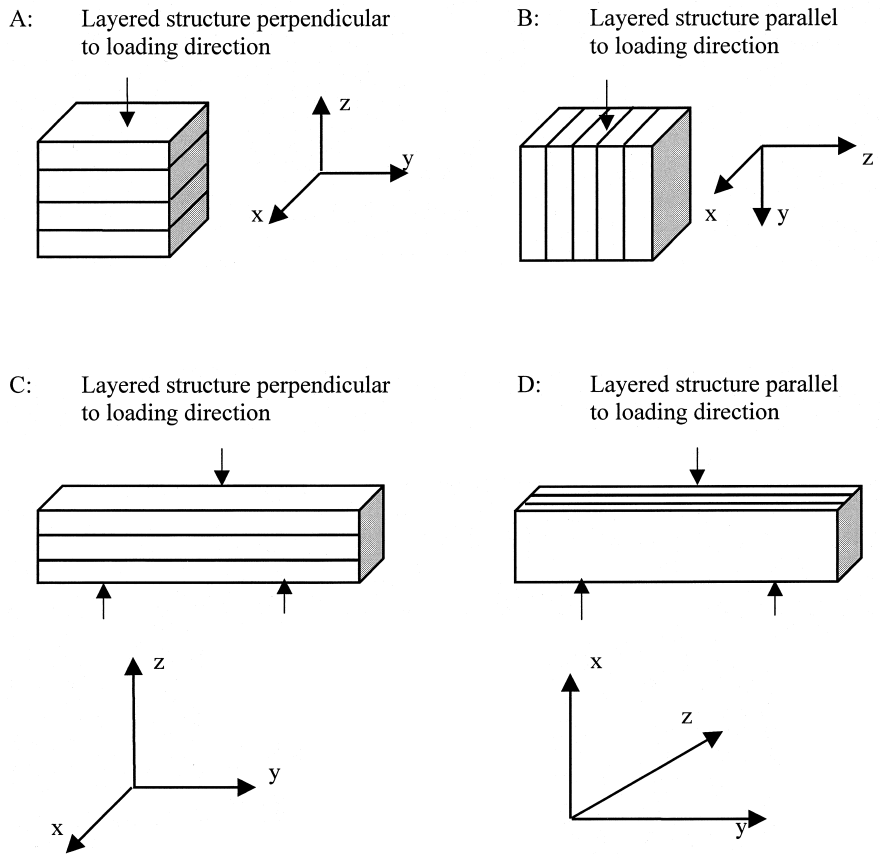

Fig. 2. Abalone compression and three-point bending configurations.

with approx. 5 mm sides. The abalone was tested parallel and perpendicular to the layered structure for both the dynamic and quasi-static compression testing. Figure 2 provides a schematic representation of the two orientations tested in compression, as well as the orientations tested in flexure. A momentum-trapped split Hopkinson [16] bar was used for the dynamic tests; details of the momentum trapping device are given elsewhere [17]. All dynamic compression tests were carried out at loading rates between 10×10^3 and 25×10^3 GPa/s.

3.2. Shear testing

Cube-shaped samples of abalone were tested as shown in Fig. 2(a) to determine the shear strength of the organic/ceramic interfaces using a shear-loading fixture shown in Fig. 3(b). The gaps s indicated in Fig. 3(a), in which the shearing action was concentrated, is equal to 2 mm. The shear strain is given by:

$$\gamma = \frac{\delta}{s} \tag{1}$$

where δ is the axial displacement. A universal testing machine was used in compression to apply the axial load after the specimen was placed in the shear device. The two blocks A and B [shown in Fig. 3(a)] were placed into a hollow tube to ensure alignment and a constant gap distance during the test. Two pins on blocks A and B were slid into grooves made in the tube in order to avoid any distortion during the test. The shear stress was obtained by dividing the load by the lateral area of the specimen.

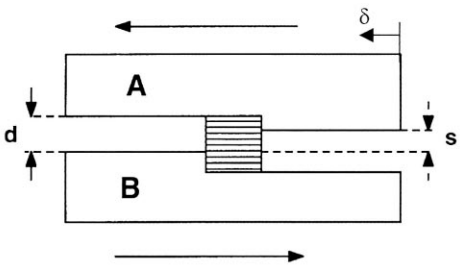

(a)

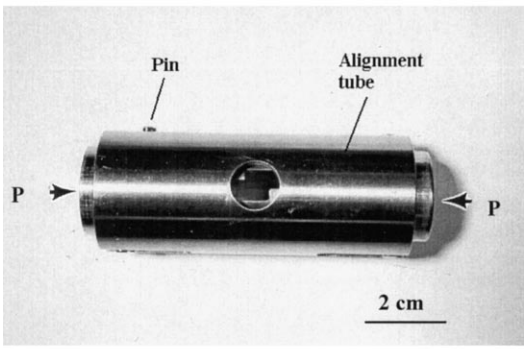

(b)

Fig. 3. (a) Sketch of the shear test configuration of the abalone shell. (b) Shear testing device.

3.3. Impact testing

In order to establish the performance and mechanisms of penetration under impact loading, ballistic experiments were performed. Square pieces were embedded in epoxy, which served as a target support. Spherical steel projectiles with a diameter of 6.3 mm were mounted in polymer sabots and accelerated by a compressed air gun. The sabots were stripped from the steel balls prior to impact by means of a steel plate containing a hole through which only the ball passed. Impacts were carried out at velocities between 160 and 300 m/s measured by magnetic sensors.

4. RESULTS AND DISCUSSION

4.1. Mechanical properties

There are many uncertainties in performing mechanical tests with mollusk shells. Besides the varying layer thickness, there are a considerable number of other natural shell irregularities such as flaws, existing microcracks or even macrocracks, and perforations made by foreign organisms. Additionally, there is some uncertainty about a given shell's history, including its age and degree of hydration. As such, the determination of the mechanical properties of these shells requires a statistical analysis in order to be quantitatively evaluated. A Weibull analysis [18] was applied to the quasi-static and dynamic compression tests by means of the following equation:

$$P(V) = \exp -(\sigma/\sigma_0)^m \tag{2}$$

where $P(V)$ is the survival probability, σ_0 and m are Weibull parameters obtained experimentally, and σ is the strength. The Weibull distribution is usually used for flexural strengths. Nonetheless, it is herein applied for compression testing, as this test configuration provided the largest amount of data. For a detailed treatment of the Weibull analysis under a variety of loading configurations, see Wachtman [19].

4.1.1. Compression and flexure testing. Figure 4(a) shows the stress–strain curves of the samples tested perpendicular to their layers (configuration A in Fig. 2). Some stress–strain curves show load drops followed by load increase. This behavior indicates the cracking of layers before a crack is temporarily arrested or deflected at other layers. The stress–strain curves after loading parallel to the layered

structure (configuration A in Fig. 2) are shown in Fig. 4(b). The maximum stresses are typically about 200 MPa, although one of the samples shows an unexpected high maximum stress of 540 MPa. The results of dynamic compression tests of abalone with layers perpendicular and parallel to the loading direction are given in Figs 4(c) and (d), respectively. The failure strains (both static and dynamic) are higher in the direction perpendicular to the layers; this is a consequence of the higher strength for this loading direction.

The results of the Weibull analyses for the two loading configurations are shown in Figs 5(a) and (b) for quasi-static and dynamic rates, respectively. Fracture probability of 50% [$P(V)=0.5$] is reached at 235 MPa with the layered structure parallel (configuration B) to the load and at 540 MPa with the layered structure perpendicular to the load (quasi-static). The Weibull parameters m are equal to 3.5 (parallel to layers; configuration B) and 2.5 (perpendicular to layers; configuration A). The 50% fracture probabilities from dynamic compression testing are 548 MPa, with the layers parallel to the loading direction (configuration B), and 735 MPa with the

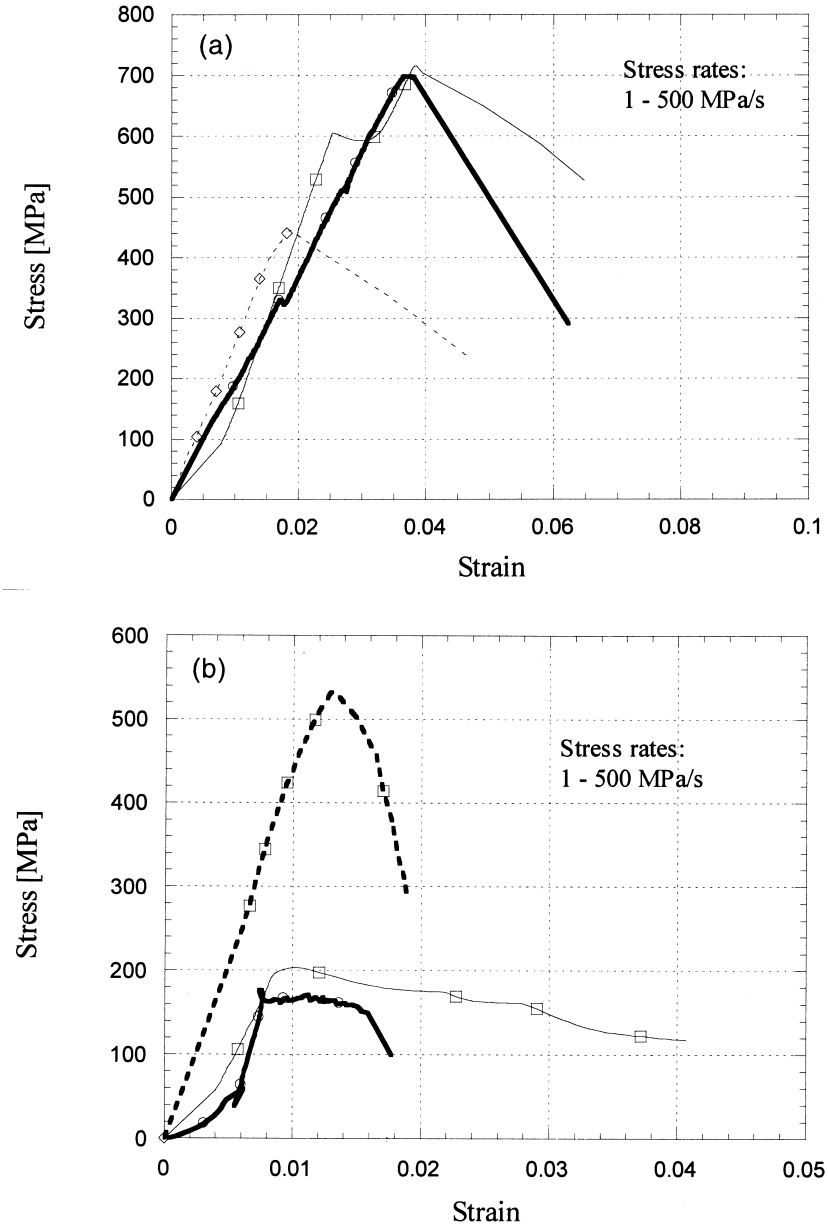

Fig. 4. Compressive stress–strain curves of abalone samples: (a) quasi-static, loading perpendicular to layered structure (configuration A); (b) quasi-static, loading parallel to layered structure (configuration B); (c) dynamic, loading perpendicular to layered structure (configuration A); (d) dynamic, loading parallel to layered structure (configuration B).

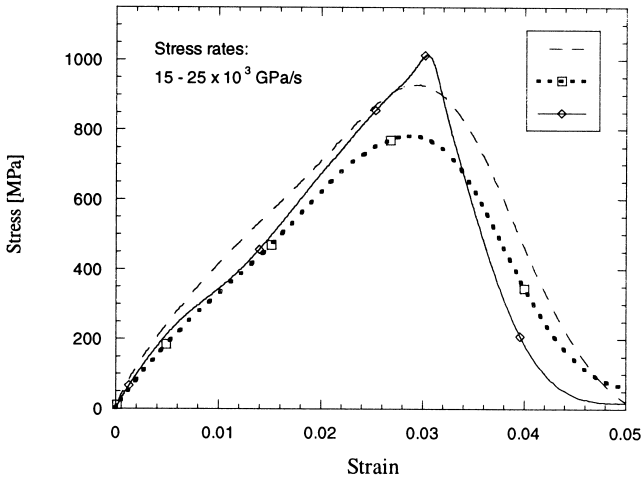

(c)

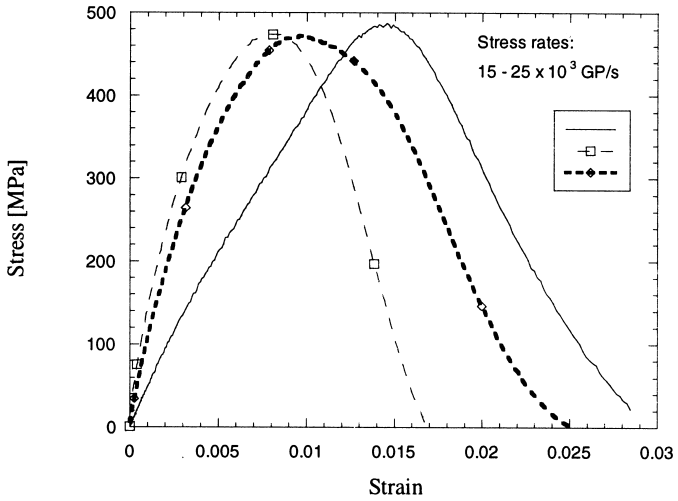

(d)

Fig. 4 (*continued*)

layered structure perpendicular to the load (configuration A). Thus, the abalone shell is stronger with layers perpendicular to the loading direction. The dynamic strength of abalone is approx. 50% higher than its quasi-static strength. Three- and four-point bending tests were also performed with the loading direction oriented both parallel (configuration D) and perpendicular to the layers (configuration C). The average bending stresses were 177 and 197 MPa for parallel and perpendicular orientations, respectively. There was no significant effect of stress rate or orientation. A very important conclusion can be drawn from the comparison of the compression and flexure strengths: the compressive strength (perpendicular to the layers) is 1.5 times the tensile strength (measured by bending tests). This is surprising: monolithic ceramics have compressive strengths that are 8–15 $\times$ their tensile strength. Another interesting phenomenon (analyzed in Section 4.2) was observed: microplastic buckling, also called kinking, takes place, to accommodate the elastic energy. This kinking reduces the compressive strength, contributing to the surprisingly low strength differential.

4.1.2. Shear strength testing. Six specimens were tested in shear, as described in Section 3, and an average shear strength of 29 ± 7.1 MPa was found. Figure 6 shows two representative stress–strain curves. The elastic region ends at about 12 MPa and is followed by a steady increase until the maximum shear strength is reached. The maximum shear strain is approx. 0.45.

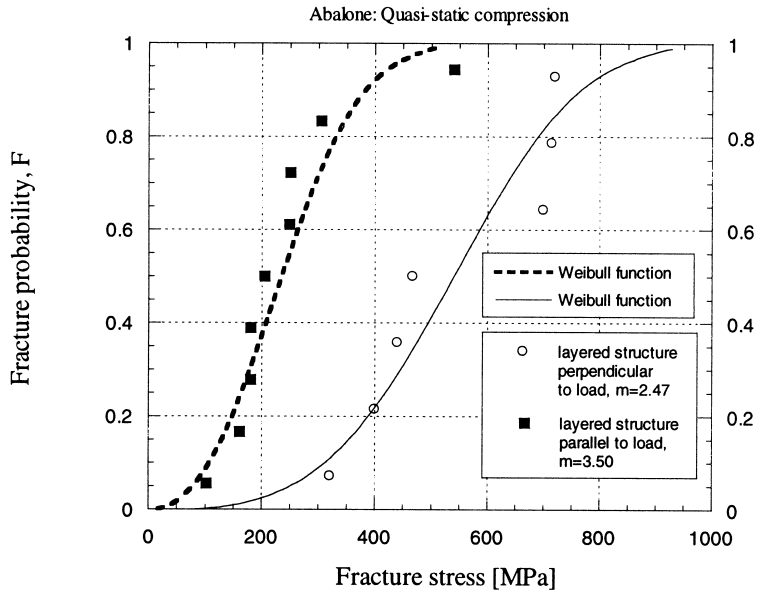

(a)

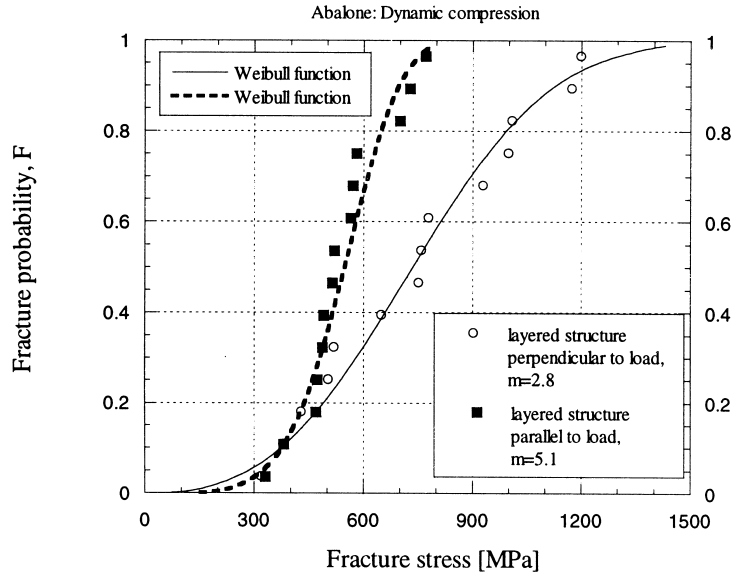

(b)

Fig. 5. Weibull distribution of compressive strength of abalone: (a) quasi-static; (b) dynamic testing.

4.2. Characterization of damage

Figure 7(a) shows the top surface of an abalone compression sample tested with the layers parallel to the load (configuration B). Cracks initiate first at the mesolayers (see arrows). Observation of the fracture surface at higher magnification reveals the fracture path in the region between the mesolayers seen in Fig. 1(a). The microlayers consist of hexagonal "tiles" shown in Fig. 7(b). A highly tortuous fracture surface of the nacre is visible. Tortuosity is one of the toughening mechanisms proposed by Sarikaya [1]. The abalone compression samples usually fragmented into many pieces during the test.

Figure 8 shows SEM micrographs at two magnifi-

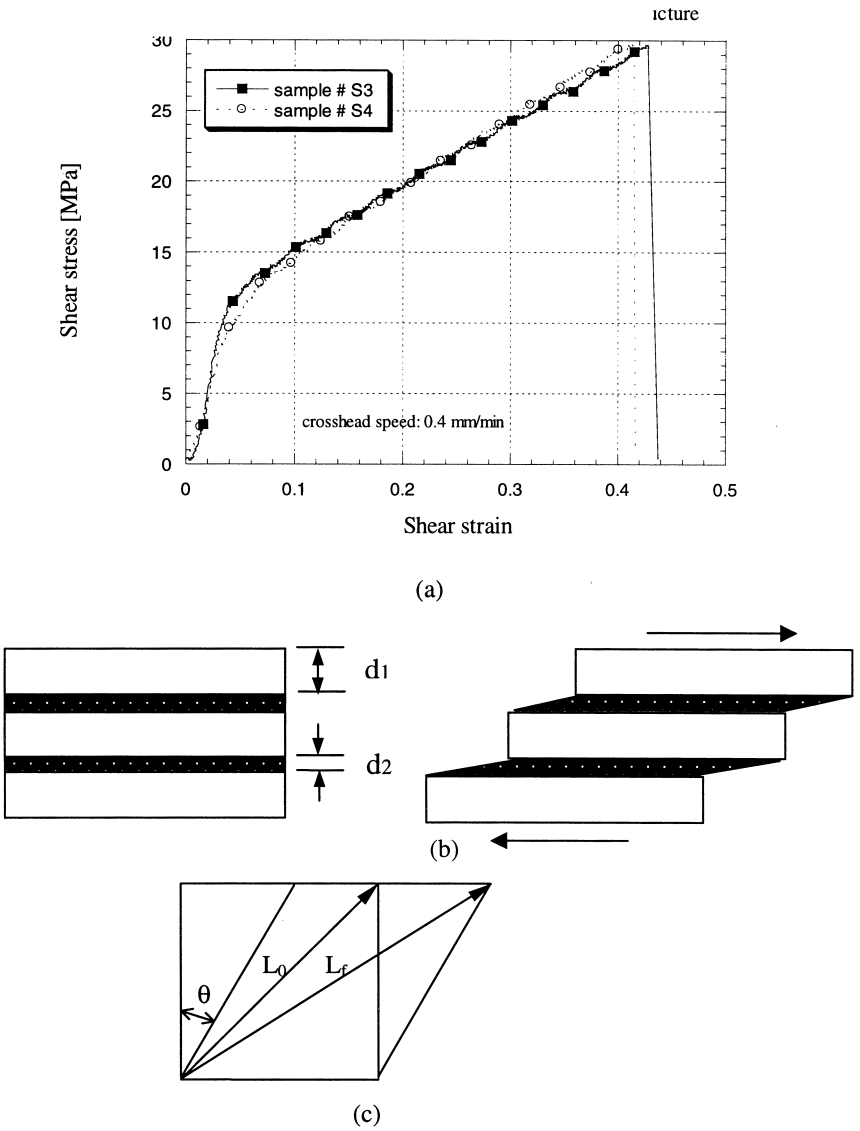

Fig. 6. (a) Stress–strain curves of abalone samples after shear strength testing of the organic/ceramic interface; (b) schematic representation of shear deformation of abalone, consisting of rigid $CaCO_3$ blocks and viscoplastic glue; (c) relationship between shear and tensile deformation.

cations from the tension portion of failure of a bending specimen. The fracture path is clearly very tortuous, and pullout of the individual platelets is evident. The fracture path occurs along the viscoplastic boundaries between the platelets. The inclined lines marked by arrows in Fig. 8(a) show that the platelets are stacked in a regular pattern, in which every second or third layer is exactly supposed. This regular stacking is due to the growth mechanism for the platelets, as discussed by Sarikaya [20]. Most of the individual platelets are intact and not fractured, indicating that failure occurred by shear of the organic layers.

An important phenomenon that was observed in a significant fraction of the specimens is the formation of plastic microbuckling as a mechanism to decrease the overall strain energy. Plastic microbuckling is a common occurrence in the compressive failure of fiber-reinforced composites when loading is parallel to the fibers. The coordinated sliding of layer segments of the same approximate length by a shear strain γ produces an overall rotation of the specimen in the region with a decrease in length. Figure 9 shows two characteristic microbuckling regions. The angle α was measured and found to be in the range 20–35° (see Fig. 9). Five measurements yielded angles of 22, 28, 30, 32, and 34°. This is consistent with the calculations by Budiansky [24] for $E/G = 2$. They report calculated values for α between 17 and 35°, at low values of the kinking failure stress. They state that kink angles α outside $10° < \alpha < 35°$ should be very infre-

quent. This is corroborated by experimental observations reported by Fleck *et al.* [26]. The ideal angle α for facilitating microbuckling is, according to Argon [23], 45°. The angle θ (rotation inside the kink band) is approx. 25° in Fig. 9(a) and 15° in Fig. 9(b) and is determined by the interlamellar sliding. This angle is consistent with the shear strain between lamellae of 0.45 observed in Fig. 6. The shear strain associated with the rotation θ in Fig. 9(a) is $\tan\theta = \gamma = 0.47$ and in Fig. 9(b) $\tan\theta = \gamma = 0.27$. Hence, the rotation θ in kinking is limited by the maximum shear strain, equal to 0.45. If this kinking rotation were to exceed 0.45, fracture along the sliding interfaces would occur.

It is possible to estimate the shear strain undergone by the organic layers prior to failure. The shear strain γ_0 in the organic layer can be found from the shear experiments reported in Fig. 6(a). This is done assuming that the $CaCO_3$ blocks remain rigid, and that all visco-elastic deformation is concentrated in the organic layers [Fig. 6(b)]. The shear strain γ is related to γ_0 by:

$$\gamma_0 = \gamma/f \tag{3}$$

where f is the fraction of organic layer, equal to the ratio [Fig. 6(b)]

$$f = \frac{d_2}{d_1 + d_2}. \tag{4}$$

From Figs 1(a) and (c), one obtains an approximate value of $f = 0.05$ ($d_1 \sim 0.4$ μm and $d_2 \sim 0.02$ μm). The organic layers are approx. 5% of the overall thickness. Taking $\gamma = 0.44$, one obtains a shear strain, in the organic layer, of $\gamma_0 \cong 0$. Sarikaya *et al.* [21], on the other hand, measured the stretching of the organic layers perpendicular to the $CaCO_3$ bricks. This is quite a different state of stress (uni-

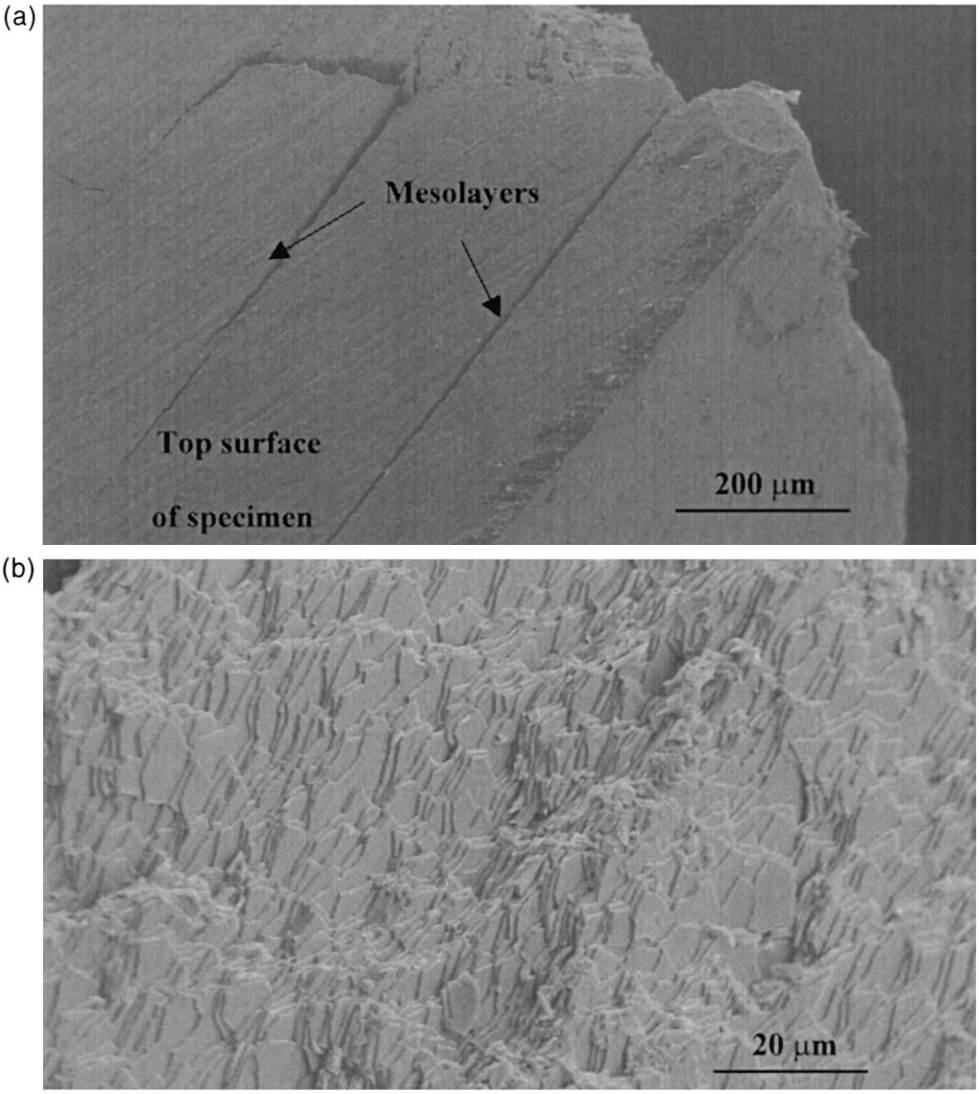

Fig. 7. Abalone compression sample, parallel direction (configuration B): (a) top surface; (b) side view.

axial stress vs simple shear) and Fig. 3 of Sarikaya *et al.* [21] shows thinning and necking of the organic ligaments, prior to failure. Nevertheless, it is instructive to compare the two strains, by converting the extensional strain reported by Sarikaya [20] into a shear strain. Figure 6(c) shows the relationship between ΔL $(=L_f - L_0)$ and $\gamma = \tan\theta$. The exact relationship is, for engineering strains (necessary for large strains):

$$\varepsilon = (1 + \gamma + \gamma^2/2)^{1/2} - 1. \quad (5)$$

Using $\gamma = 9$, one obtains $\varepsilon = 6.1$. This value is reasonably close to the value reported by Sarikaya *et al.* [21]: up to 10. The visco-elastic response of the organic layer is obviously dependent on the degree of hydration. The measurement reported by Sarikaya *et al.* [21] is based on SEM observations. Considering the differences in materials, testing methods, and stress states, the agreement is reasonable.

Similar features, as discussed above for the mechanical tests, were observed in the specimen subjected to impact by a spherical projectile. The lenticular features seen in Figs 10(a) and (b) resemble deformation twins, but are actually kink bands. The thickness of these kink bands is considerably less than those formed quasi-statically. The kink bands seen in Fig. 9 have a thickness of approx. 100 μm, whereas the kink bands formed in ballistic impact [Fig. 10(b)] have a thickness of approx. 20 μm. The smaller scale of the kink bands formed under ballistic impact may be responsible for their lenticular shape observed in some cases. The kink bands terminate within a single mesolayer and their extremities are sharp [see arrows in Fig. 10(b)]. In quasi-static testing, on the other

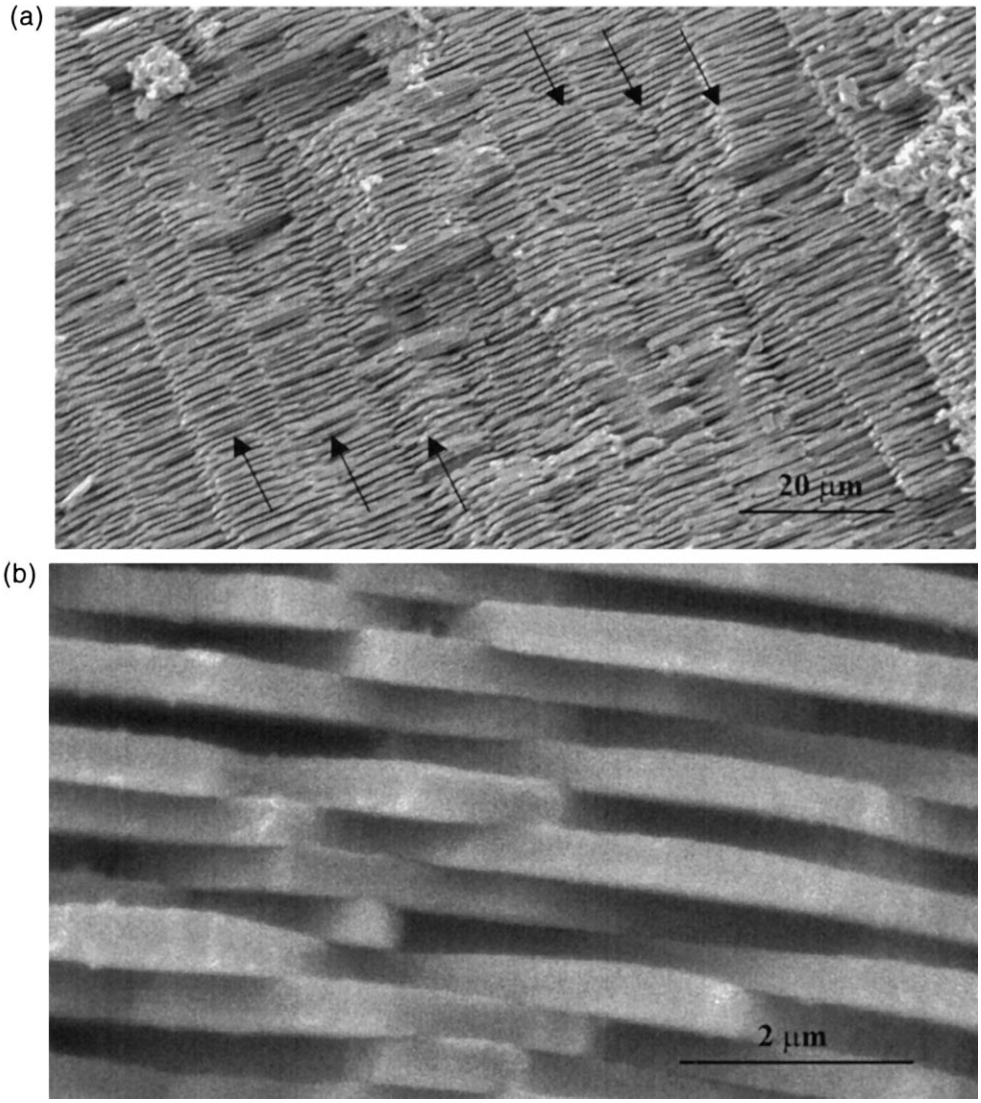

Fig. 8. Failure of abalone in bending test: (a) lower magnification; (b) higher magnification, showing intact platelets, failure occurring by pullout.

hand, kink bands extend over several macrolayers, as shown in Fig. 9. Similar features were observed by Espinosa *et al.* [22] in laminated composites subjected to penetration by projectiles.

Argon [23] developed a formalism for the calculation of the compressive strength of laminates, which is based on kinking, or plastic microbuckling. The plastic work done inside the band (W) is equated to elastic energy stored at the extremities of the band (ΔE_1) and elastic energy outside the band that opposes its expansion (ΔE_2). By using the equality ($\Delta E_1 + \Delta E_2 - W = 0$), the strength of the composite is obtained:

$$\sigma \cong \frac{\tau}{\theta_0}\left[1 + \frac{bG_c\Delta\theta}{2\pi a\tau(1-\nu)}\ln\left(\frac{2\pi a\tau(1-\nu)}{bG_c\Delta\theta}\right) + \frac{E_r\Delta\theta}{48\tau}\left(\frac{t_r}{b}\right)^2\right] \quad (6)$$

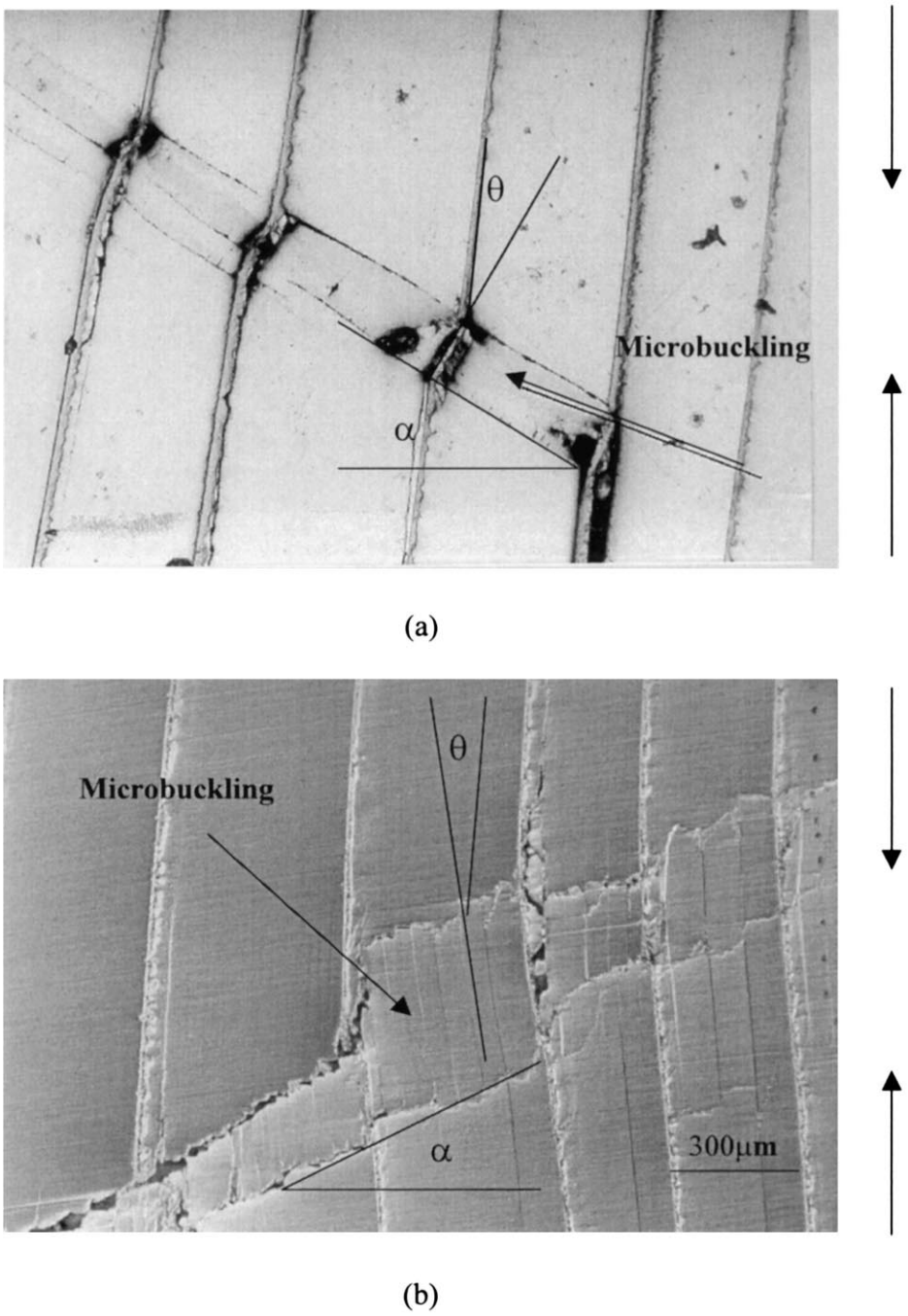

Fig. 9. Microbuckling observed in compression testing of abalone specimens (configuration B).

where τ is the shear strength of the matrix, θ_0 is the angle between the reinforcement and the loading axis [see Fig. 11(a)], E_r is Young's modulus of the reinforcement, t_r is the lamella thickness, G_c is the shear modulus of the composite, ν is Poisson's ratio, and a and b are the kink nucleus dimensions. When $\Delta\theta \to 0$, at the onset of collapse, the second and third terms in equation (6) reduce to zero and the equation simplifies itself to:

$$\sigma \cong \frac{\tau}{\theta_0} \tag{7}$$

This analysis has been further developed by Budiansky [24], Evans and Adler [25], Fleck *et al.* [26], Jelf and Fleck [27], and Dao and Asaro [28]. Budiansky [24] derived the following expression:

$$\sigma = \frac{\tau\left[1 + (\sigma_{Ty})^2 \tan^2 \alpha\right]}{\theta_0 + \Delta\theta} \tag{8}$$

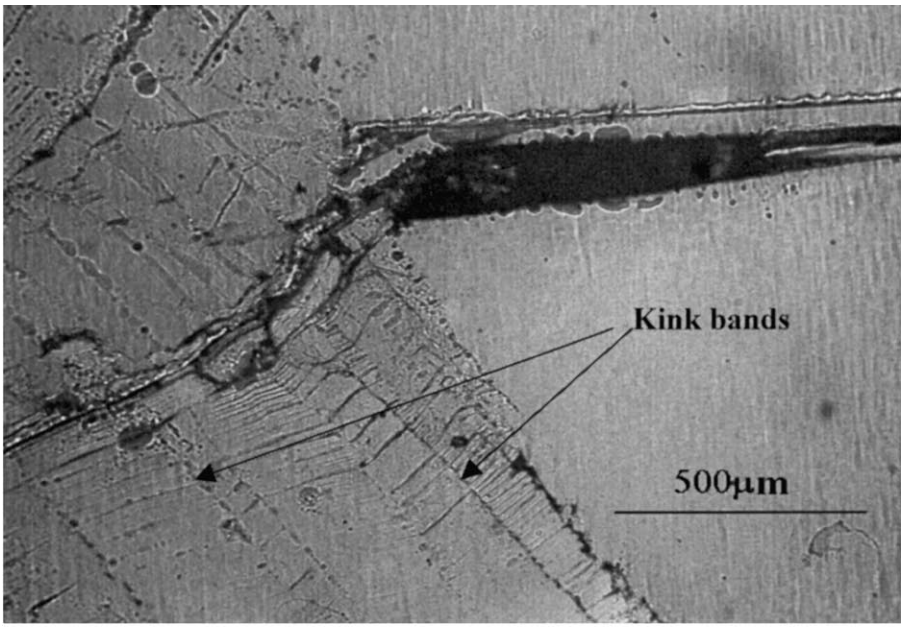

(a)

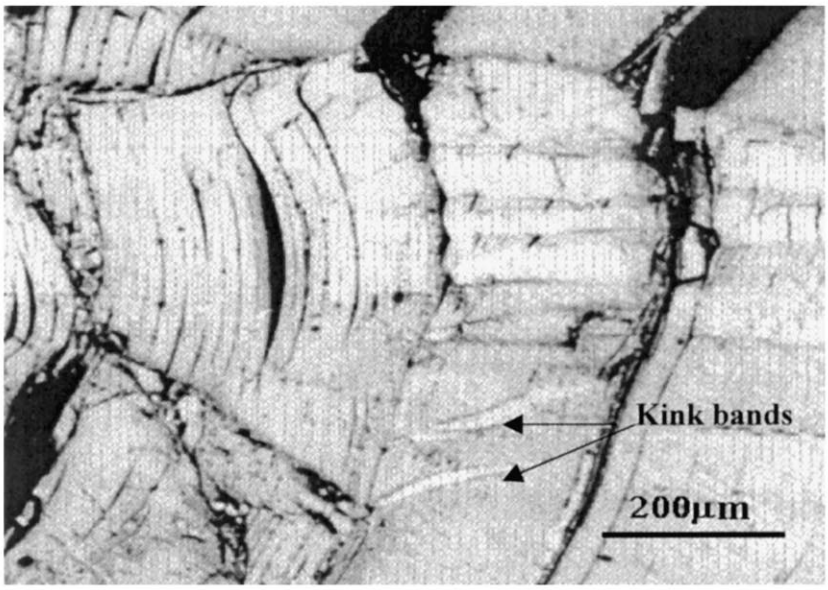

(b)

Fig. 10. Abalone shell after ballistic impact; kink banding (microbuckling) and delamination at microlevel.

where σ_{Ty} is the transverse tensile strength of the composite. When the angle between the kink band and the normal to the compressive axis is zero (i.e. $\alpha = 0$), it reduces itself to Argon's equation (8), at the onset of microbuckling ($\Delta\theta = 0$). The resolved shear stress along the organic glue layers, produced by the compressive stress σ_c, is also simply given by the Schmid equation (resolved shear stress along the slip plane and slip direction):

$$\tau_y = \sigma_c \cos\theta_0 \cos(\pi/2 - \theta_0) = \sigma_c \cos\theta_0 \sin\theta_0. \quad (9)$$

This leads to the following approximate relationship for the compressive strength of the composite, valid at small angles θ_0 (stress at which viscoplastic flow along the organic layers is initiated, leading to kinking):

$$\sigma_c \cong \frac{\tau_y}{\theta_0}. \quad (10)$$

This is equation (13) from Budiansky [24] and equation (A-7) from Argon [23]. Equation (10) assumes that the fiber material is brittle and that the elastic bending of fibers, θ, is small with respect to θ_0. There is no limitation in the volume fraction of reinforcement in equation (10); thus, the Argon [23] and Budiansky [24] equations can, in principle, be applied to abalone, in which the brittle phase is 95% of the total volume.

Budiansky [24] extended the treatment using a perturbation analysis and obtained an estimate for the thickness of the kink bands, w, in terms of the spacing between the reinforcement units, d. For brittle fibers, this is:

$$\frac{w}{d} = \frac{\pi}{4}\left(\frac{2\tau_y}{CE}\right)^{-1/3}. \quad (11)$$

E is the Young's modulus of the fibers and C is

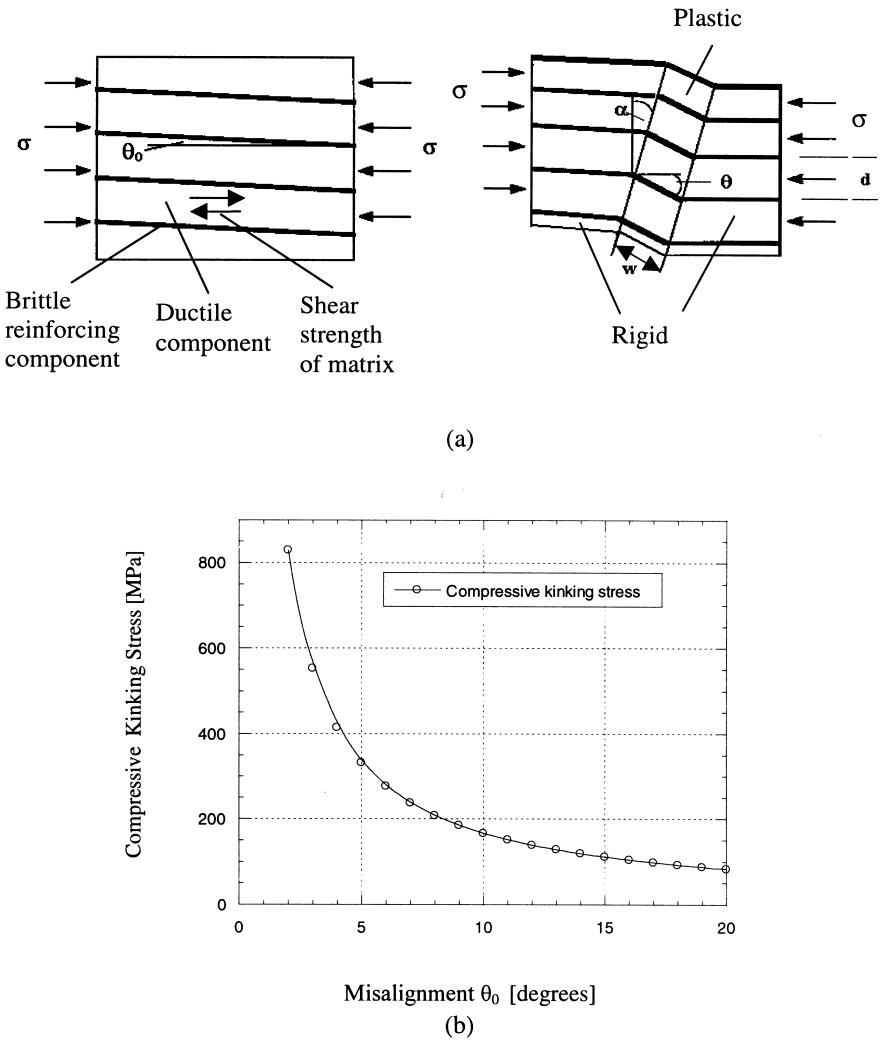

Fig. 11. (a) Schematic configuration for Argon mechanism of plastic microbuckling; (b) theoretical compressive strength for abalone; different misalignment angles between loading and layer directions (organic layer strength: 29 MPa).

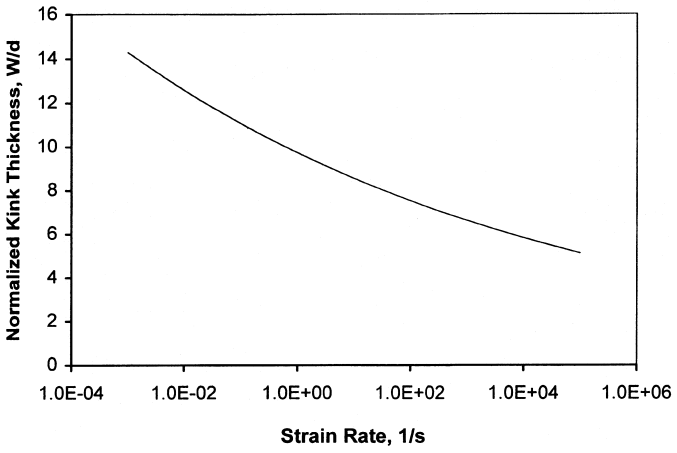

(a)

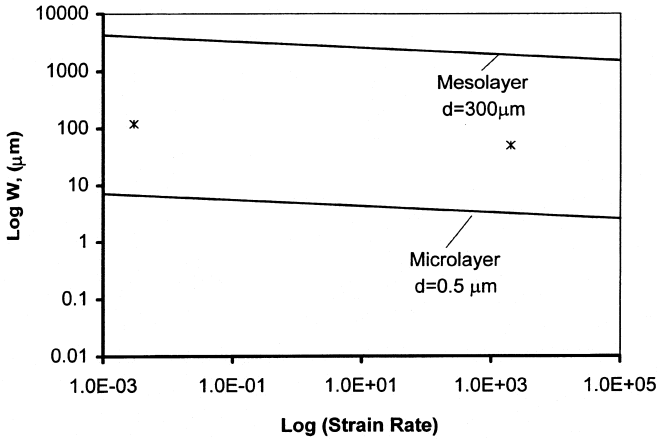

Fig. 12. (a) Budiansky [24] equation prediction of kink-band thickness/reinforcement spacing ratio (w/d), as a function of strain rate; (b) predicted and experimentally measured kink-band thickness considering meso- and micro-layer as the spacing.

their volume fraction. It is interesting to note that equation (11) predicts a decrease in w/d with increasing τ_y. It is possible to predict the effect of the strain rate on w. Gray *et al.* [29] investigated the effect of strain rate on the mechanical response of Adiprene L-100, a polyurethane-based rubber. This material, and other polymers and rubbers, exhibits a high strain-rate sensitivity, and the flow stress increases from 0.5 MPa at 0.001 s^{-1} to 6 MPa at 3000 s^{-1}. This response can be expressed as:

$$\sigma = A\dot{\varepsilon}^m = 1.57\dot{\varepsilon}^{0.17} \quad \text{(in MPa)}. \tag{12}$$

For the organic glue, changing the pre-exponential factor to B in order to fit the experimental results for abalone:

$$\frac{w}{d} = \frac{\pi}{4}\left(\frac{B\dot{\varepsilon}}{CE}\right)^{-1/3}. \tag{13}$$

For the purpose of this work, the analysis by Argon will suffice and equation (7) will be employed. In the case of the abalone with compressive loading along the layers, the shear strength of the matrix is replaced by the strength of the organic layer. Figure 11(b) shows a plot of the calculated compressive kinking stress as a function of misalignment θ_0. It is clear that it is critically dependent on θ_0 and that, within the misorientations found experimentally, one can obtain a wide range of stresses. Indeed, θ_0 values up to 10° are normal in the specimens tested, and the corresponding range of kinking stress from Fig. 11(b) (from 175 MPa for 10° to 820 MPa for 2.5°) is consistent with the experimentally observed values (see Fig. 5).

Figure 12(a) shows the predicted values of w/d. The Young's modulus is taken from Jackson *et al.* [11] and is equal to approx. 60 GPa; $C = 0.95$ (the fraction that is comprised by the reinforcement). B is taken as 30 MPa [the flow stress at a shear strain

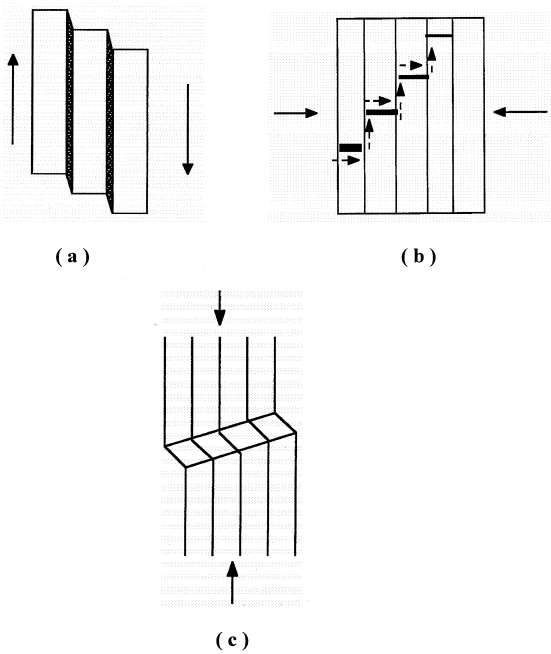

Fig. 13. Principal mechanisms of damage accumulation in shells: (a) viscoplastic deformation of organic layers; (b) crack deflection by organic layers; (c) plastic microbuckling (kinking) under compressive loading.

of $\gamma = 0.02$ in Fig. 6(a)]. In Fig. 12(b), the spacing between reinforcements is introduced. Two scales, shown in Fig. 1, are considered: (a) the thickness of the microscopic "bricks", that is equal to 0.5 μm; and (b) the spacing between mesolayers, that is equal to 300 μm. It is interesting to observe that the experimental results [marked * in Fig. 12(b)] are approximately halfway between the meso- and microlayers. This is entirely consistent with the observation of the kinked structure. These regions show the formation of columns having a thickness that is intermediate between 0.5 and 300 μm [Figs 9(b) and 10(a)]. The slip is concentrated on layers with a thickness intermediate between the micro- and meso-layers. Another important aspect of Fig. 12(b) is that the predicted and experimentally observed strain-rate dependencies of kink-band thickness w are consistent. Thus, Budiansky's formalism correctly predicts the strain-rate dependence of kink thickness, w.

4.3. Damage mechanisms

From the above observations and analysis, it is apparent that the shell structure imparts a significant increase in the toughness of an otherwise brittle monolithic material ($CaCO_3$). Two primary toughening mechanisms were identified: (a) sliding of $CaCO_3$ blocks by means of viscoplastic deformation of the organic interfacial layers [Figs 13(a) and (b)] arrest; and deflection of cracks by the viscoplastic layers [Fig. 13(b)]. These two basic mechanisms and the fine microstructure, consisting of $CaCO_3$ platelets, lead to delocalization of failure, by which one single sharp crack is replaced by a large number of smaller cracks, within a broader region. A corollary of the viscoplastic deformation is the formation of kink bands in compressive loading of the abalone shells in the direction parallel to the lamellae [Fig. 13(c)]. It is of interest, and will serve as the basis of further study, to determine in a quantitative manner the amount of energy which can be dissipated by each of these toughening mechanisms.

5. SUMMARY AND CONCLUSIONS

Mechanical tests were carried out over a range of stress rates and stress states to assess the mechanisms of damage accumulation in an abalone shell. The strength of this shell shows a considerable variation, and is well represented by a Weibull distribution with parameter m varying between 2.5 and 6.8. The quasi-static compressive strengths [$P(V) = 0.5$] are on the order of 540 and 235 MPa for loading perpendicular and parallel to the layered structures (configurations A and B in Fig. 2), respectively, and the tensile strength obtained from flexural tests is about 180 MPa. This is a surprisingly low ratio between compressive and tensile strength (1.5–3), considerably below that of monolithic ceramics (8–12). This difference is attributed to delamination and kinking in compression. The dynamic compressive strength is approx. 50% higher than the quasi-static value. It can be concluded that the hierarchical structure of this shell enhances its toughness in a significant fashion, by providing three important mechanisms for controlling damage: (a) viscoplastic deformation of organic layers; (b) crack deflection by organic layers; and (c) plastic microbuckling under compressive loading.

Acknowledgements—This research was partially supported by the US Army Research Office under the MURI program (Contract No. DAAHO4-96-10376). R. Menig worked at UCSD as part of an exchange program between the University of Karlsruhe (TH) and the University of California, San Diego. Appreciation is extended to Otmar Vöhringer for making this exchange possible. We would like to thank David Harach and Y.-J. Chen for setting up the quasi-static test configurations and A. Strutt for his assistance in the SEM analysis. G. Ravichandran, of the California Institute of Technology, kindly allowed us to use his laboratory to perform some of the quasi-static compression, flexural, and shear tests; his help and that of his student, S. Zhuang, is gratefully acknowledged. We would like to thank G. Mayer (US ARO) for having stimulated our interest in this topic and M. Sarikaya (University of Washington) for insightful discussions.

REFERENCES

1. Sarikaya, M., *Microsc. Res. Techn.*, 1994, **27**, 360.
2. Srinivasan, A. V., Haritos, G. K. and Hedberg, F. L., *Appl. Mech. Rev.*, 1991, **44**, 463.
3. Vincent, J. F. V., *Structural Biomaterials*. Princeton University Press, Princeton, NJ, 1991.
4. Baer, E., Hiltner, A. and Morgan, R. J., *Phys. Today*, Oct. 1992, 60.
5. Lowenstam, H. A. and Weiner, S., *On Biomineralisation*. Oxford University Press, New York, 1989.
6. Vincent, J. F. V. and Owers, P., *J. Zool. Lond. (A)*, 1986.
7. Laraia, J. V. and Heuer, A. H., *J. Am. Ceram. Soc.*, 1989, **72**, 2177.
8. Kuhn-Spearing, L. F., Kessler, H., Chateau, E., Ballarin, R. and Heuer, A. H., *J. Mater. Sci.*, 1996, **31**, 6583.
9. Weiner, S., *Am. Zool.*, 1984, **24**, 945.
10. Currey, J. D. and Kohn, A. J., *J. Mater. Sci.*, 1976, **11**, 1614.
11. Jackson, A. P., Vincent, J. F. V. and Turner, R. M., *Proc. R. Soc. Lond. B*, 1988, **234**, 415.
12. Sarikaya, M., Gunnison, K. E., Yasrebi, M. and Aksay, J. A., *Materials Research Society, Pittsburgh, PA*, 1990, **174**, 109.
13. Currey, J. D., *Proc. R. Soc. Lond. B*, 1977, **196**, 443.
14. Sarikaya, M. and Aksay, J. A., in *Results and Problems in Cell Differentiation in Biopolymers*, ed. S. Case. Springer, Amsterdam, 1992, p. 1.
15. Meyers, M. A., *Mechanical Behavior of Materials*. Prentice-Hall, Upper Saddle River, NJ, 1999, p. 41.
16. Kolsky, H., *Proc. R. Soc. B*, 1949, **62**, 676.
17. Nemat-Nasser, S., Isaacs, J. B. and Starrett, J. E., *Proc. R. Soc. A*, 1991, **435**, 371.
18. Weibull, W., *Ingenioersvetenskapsakad. Handl.*, 1939, **151**, 1.
19. Wachtman, J. B., *Mechanical Properties of Ceramics*. Wiley–Interscience, New York, 1996.
20. Sarikaya, M., Personal communication, 1997.
21. Sarikaya, M., Gunnison, K. E., Yasrebi, M., Milius, D. L. and Aksay, I. A., in *Biotechnology and Composite Materials, Am. Soc. Comp. Proc. Fifth Tech. Conf., Technomic, Lancaster, PA*, 1990, p. 176.
22. Espinosa, H. D., Hung-Cheng, L. and Yueping, X., *J. Comp. Mater.*, 1998, **32**, 722.
23. Argon, A. S., in *Treatise of Materials Science and Technology*. Academic Press, New York, 1972, p. 79.
24. Budiansky, B., *Comput. Struct.*, 1983, **16**, 3.
25. Evans, A. G. and Adler, W. F., *Acta metall.*, 1977, **26**, 725.
26. Fleck, N. A., Deng, L. and Budiansky, B., *J. appl. Mech.*, 1995, **62**, 329.
27. Jelf, P. M. and Fleck, N. A., *J. Comp. Mater.*, 1992, **26**, 2701.
28. Dao, M. and Asaro, R. J., *Scripta mater.*, 1996, **34**, 1771.
29. Gray III, G. T., Blumenthal, W. R., Trujillo, C. P. and Carpenter II, R. W., *J. Phys. IV, France*, 1997, **7**, C3.